Chemical Science

Accepted Manuscript

This article can be cited before page numbers have been issued, to do this please use: C. Yang, R. Mu, G. Wang, J. Song, H. Tian, Z. Zhao and J. Gong, *Chem. Sci.*, 2019, DOI: 10.1039/C8SC05608K.

View Article Online
DOI: 10.1039/C8SC05608K

Chemical Science

ARTICLE

# Hydroxyl-mediated ethanol selectivity of $CO_2$ hydrogenation

Chengsheng Yang[1], Rentao Mu[1], Guishuo Wang, Jimin Song, Hao Tian, Zhi-Jian Zhao, and Jinlong Gong*

Received 00th January 20xx,
Accepted 00th January 20xx

DOI: 10.1039/x0xx00000x

**www.rsc.org/**

Oxide-supported Rh nanoparticles have been widely used for $CO_2$ hydrogenation, especially for the ethanol synthesis. However, this reaction operates under high pressure up to 8 MPa and suffers low $CO_2$ conversion and alcohols selectivity. This paper describes the crucial role of hydroxyl groups bound on Rh-based catalysts supported on $TiO_2$ nanorods (NRs). The RhFeLi/$TiO_2$ NRs catalyst shows superior reactivity (≈15% conversion) and ethanol selectivity (32%) for $CO_2$ hydrogenation. The promoting effect can be attributed to the synergism of high Rh dispersion and high-density hydroxyl groups on $TiO_2$ NRs. Hydroxyls are proven to stabilize formate species and protonate methanol, which is easily dissociated into $^*CH_x$, and then $^*CH_x$ is inserted by CO obtained from the reverse water-gas shift reaction (RWGS) to form $CH_3CO^*$, followed by $CH_3CO^*$ hydrogenation to ethanol.

## Introduction

Carbon dioxide ($CO_2$) is one of the major components of greenhouse gases, which can result in climate change and ocean acidification. Among the different approaches explored for controlling $CO_2$ emission, the chemical conversion of $CO_2$ to high-value-added fuels (oxygenates, alcohols, and olefin *et al.*) has attracted extensive attention.[1-4] Compared with $C_1$ product (CO, $CH_4$ and $CH_3OH$), the higher alcohols ($C_{2+}OH$, especially $C_2H_5OH$), which are mostly produced from biological fermentation, have been widely applied in industries as indispensable higher-energy-densities engine fuel and fuel additive.[1] According to the thermodynamic analysis, the formation of ethanol from $CO_2$ is limited enormously at 1-30 bar due to the preferential production of CO or $CH_4$, thus the selectivity of ethanol is relatively low.[4]

Therefore, the production of $C_{2+}OH$ by $CO_2$ hydrogenation is appalling but remains grand challenging. Previous studies have shown that a $Pt/Co_3O_4$ catalyst[5] achieved 27.3% selectivity of $C_{2+}OH$ with $H_2O$/DMI as a solvent. Multi-functional composite catalysts, such as CoMoS[6] (5.5% selectivity of ethanol), physically mixed Fe-based and Cu-based catalysts[7] (17.4% selectivity of ethanol) and K/Cu-Zn-Fe catalysts[8,9] (19.5% selectivity of $C_{2+}OH$ and $CH_3OH$) were also used for alcohols synthesis. Particularly, Rh-based catalysts have been evaluated as promising catalysts for the selective synthesis of ethanol.[4,10-11] In general, promoters such as Fe and Li are frequently used in enhancing ethanol selectivity via changing the electronic state of Rh and increasing the intensity of bridged-bond CO species. For example, 5 wt% RhFe[10] and RhLi[11] supported on $SiO_2$ showed ethanol selectivities of 16.4% and 15.5%, respectively.

However, there are still some limitations for the alcohols production through $CO_2$ hydrogenation reaction, such as the difficulties in $CO_2$ activation, high energy barrier for C-O bond scission and the formation of $C_1$ by-products.[1] Therefore, the design of efficiently heterogeneous catalysts for ethanol production is of great importance. Tuning the particle size of noble metals can often increase the $CO_2$ conversion and product selectivity.[12-16] For example, the suitable reducible metal oxide supports, such as $TiO_2$, $ZrO_2$, have been extensively applied to tune the particle size.[17-18] The Au/$TiO_2$ catalyst with abundant oxygen vacancies exhibited high selectivity to ethanol from $CO_2$ reduction in DMF solvent.[19] Bimetallic $Pd_2Cu$/P25 catalyst also presented the excellent yield of ethanol with the help of water.[20] On the other hand, promotion strategy via hydroxyl groups has been also proved to be an efficient approach towards improving alcohols selectivity in CO hydrogenation.[21-23]

This work shows that the high yield of ethanol under low pressure can be achieved by the introduction of hydroxyls onto $TiO_2$ support. Firstly, 1wt% RhFeLi (Rh:Fe:Li =1:1:1) supported on a series of reducible oxides were prepared. The catalysts supported on $TiO_2$ nanorods (NRs) display highest selectivity of ethanol. Since $TiO_2$ NRs have been extensively used in a variety of catalytic systems, such as photocatalytic water splitting, $CO_2$ photoreduction and dissociation of $CO_2$ to CO,[24-26] we synthesized $TiO_2$ NRs by the modified hydrothermal method. More importantly, high-density surface hydroxyls can be introduced to the catalytic system after reduction of $TiO_2$ NRs-supported catalysts in $H_2$. A significant improvement of ethanol yield is observed over Rh-based catalysts supported on $TiO_2$ NRs, which have not been reported in the previous works. Furthermore, the hydroxyl-mediated mechanism of ethanol formation over RhFeLi/$TiO_2$ NRs catalysts is investigated.

---

*Key Laboratory for Green Chemical Technology of Ministry of Education, School of Chemical Engineering and Technology, Tianjin University; Collaborative Innovation Center of Chemical Science and Engineering, Tianjin 300072, China. Email: jlgong@tju.edu.cn*

† Electronic Supplementary Information (ESI) available: Details in Experimental section and supporting figures and tables. See DOI: 10.1039/x0xx00000x

DOI: 10.1039/C8SC05608K

## Results and discussion

### Catalyst structure

The morphology of synthesized $TiO_2$ NRs is shown in Fig. 1a and Fig. S1.† The length and diameter of $TiO_2$ NRs are 50-200 nm and 10-20 nm, respectively. The specific surface area of $TiO_2$ NRs is determined to be 23.6 $m^2 \cdot g_{cat}^{-1}$, which is close to that of commercial $TiO_2$ ($TiO_2$ Com, 18.2 $m^2 \cdot g_{cat}^{-1}$) (Table S1†). The Rh-based catalysts supported on $TiO_2$ NRs and $TiO_2$ Com were prepared by incipient wetness impregnation. The Rh nanoparticles on $TiO_2$ NRs present uniform size distribution with an average diameter of 2.3 ± 1.0 nm (Fig. 1a, c, e). The high-resolution images of Rh nanoparticles in Fig. 1c and 1d present a lattice distance of 0.23 nm, corresponding to Rh (111) planes.[27] In contrast, two-times-larger (~ 4.0 nm) Rh nanoparticles in the range of 1-7 nm are observed on $TiO_2$ Com (Fig. 1b, d, f). TEM studies indicate $TiO_2$ NRs can prevent the Rh nanoparticles from severe agglomeration after the reduction at 400°C in $H_2$ atmosphere.

In XRD measurements, no characteristic peak of $Fe_2O_3$ can be found over RhFeLi/$TiO_2$ Com and RhFeLi/$TiO_2$ NRs when the loading of Fe is relatively low (~ 1 wt%) (Fig. 2). When the loading of Fe is increased to 2.5 wt%, the diffraction peak of $Fe_2O_3$ at 33.2° can be seen on $TiO_2$ Com. However, diffraction peak of $Fe_2O_3$ does not appear on $TiO_2$ NRs even though the loading of Fe is increased to 5 wt% (Fig. 2). XRD results indicate that the dispersion of $FeO_x$ over $TiO_2$ NRs is higher than that over $TiO_2$ Com. EDS elemental mapping of RhFeLi/$TiO_2$ NRs also shows that $FeO_x$ species are well dispersed on $TiO_2$ NRs (Fig. 1g). We note that no Raman shift of $TiO_2$ can be observed for all catalysts (Fig. S2†), indicating $FeO_x$ species are deposited on surface rather than doping into $TiO_2$ bulk. $H_2$ temperature-programmed reduction ($H_2$-TPR) results of $FeO_x$/$TiO_2$ show that the reduction temperature of $FeO_x$ over $TiO_2$ NRs is 100°C higher than the reduction temperature of $FeO_x$ over $TiO_2$ Com (Fig. S3a †), suggesting $FeO_x$ species are better dispersed on $TiO_2$ NRs compared with $TiO_2$ Com.

$H_2$-TPR studies of RhFeLi/$TiO_2$ NRs and RhFeLi/$TiO_2$ Com were also carried out to investigate the interfacial interaction between Rh and oxide promoters (Fig. S3b†). According to previous studies,[10] the peaks below 200°C can be ascribed to the reduction of $Rh_2O_3$, while the broad peak appearing at higher temperature (300-500°C) can be assigned to the reduction of $Fe_2O_3$. We find that the reduction temperature of $Rh_2O_3$ for RhFeLi/$TiO_2$ NRs is 50°C higher than that on RhFeLi/$TiO_2$ Com, illustrating smaller Rh size on $TiO_2$ NRs.[14] As such, the higher dispersion of Rh-based nanoparticles on $TiO_2$ NRs should increase the number of interfacial sites between Rh and oxide promoters, where C-C coupling occurs via reaction between CO and $*CH_x$.[5-7]

To further illustrate the surface structure of RhFeLi/$TiO_2$ NRs and RhFeLi/$TiO_2$ Com catalysts, CO titration experiments were conducted. The active loop volume of CO for RhFeLi/$TiO_2$ Com (0.09 $cm^3/g$), which is consumed by CO adsorption on Rh, is much smaller than that for RhFeLi/$TiO_2$ NRs (0.69 $cm^3/g$) (Table S2 † ). The observed low adsorption amount of CO on RhFeLi/$TiO_2$ Com may be due to the partially encapsulation of Rh sites by oxide overlayers. TEM image also shows the Rh nanoparticles are decorated by oxide overlayers over RhFeLi/$TiO_2$ Com catalyst (Fig. 1d). Quantitative XPS analysis was also conducted to investigate the surface structure of Rh-based catalysts (Table S3†). The surface molar ratio of Rh:Fe

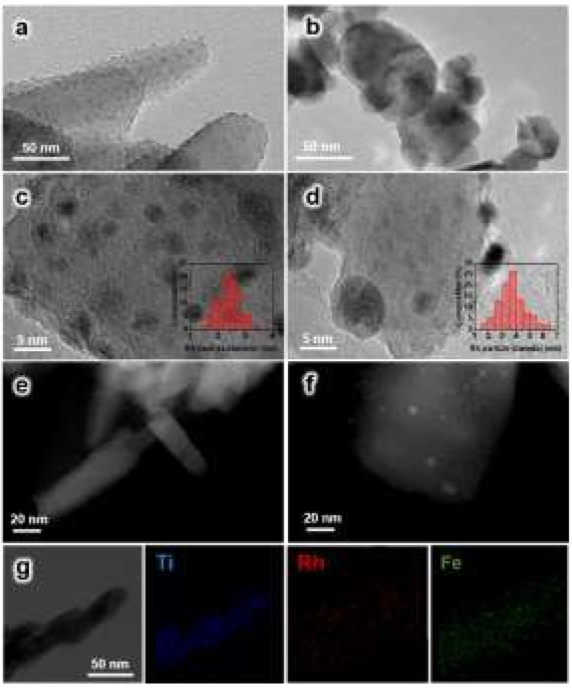

**Fig. 1.** (a, b) TEM; (c, d) HRTEM images, particle size distributions (Inset figures) and (e, f) HAADF-STEM images of catalysts after reaction. 2.5 wt% RhFeLi supported on $TiO_2$ NRs (a, c, e), 2.5 wt% RhFeLi supported on $TiO_2$ Com (b, d, f). (g) STEM-EDS elemental map of 2.5 wt% RhFeLi supported on $TiO_2$ NRs.

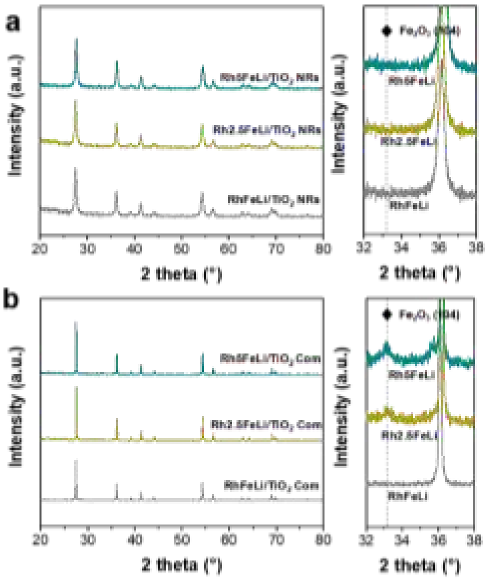

**Fig. 2.** (a) XRD spectra of 2.5 wt% RhFeLi/$TiO_2$ NRs with different Fe loadings. (b) XRD spectra of 2.5 wt% RhFeLi/$TiO_2$ Com with different Fe loadings. The Figures on right of (a) and (b) show the enlarged XRD patterns.

over RhFeLi/$TiO_2$ NRs is determined to be 58:42, which is close to the bulk molar ratio of Rh:Fe measured by ICP-AES (48:52) and the initial feed ratio. For RhFeLi/$TiO_2$ Com, XPS investigations show that the surface molar ratio of Rh:Fe is 29:71. However, the bulk molar ratio of Rh:Fe determined by ICP-AES (Rh:Fe = 50:50) still agrees with the initial feed ratio, suggesting the Rh nanoparticles should be partially covered by $FeO_x$ species. Note that the binding energy (BE) of Rh $3d_{5/2}$ locates at ~ 307.0 eV (Fig. S4b†), corresponding to the metallic state of Rh.[28]

### Catalytic performance

The catalytic performance to $CO_2$ hydrogenation is studied over Rh-based catalysts supported on different oxide supports. The $TiO_2$ NRs-supported catalysts present highest ethanol yield (Fig. S5†). Additionally, a series of Rh-based catalysts with different promoters were synthesized. Compared with mono-component Rh/$TiO_2$ catalyst, the selectivity of ethanol over RhFe/$TiO_2$ is improved significantly (16% for RhFe/$TiO_2$ Com and 25% for RhFe/$TiO_2$ NRs in Fig. S6†). With the loading of Fe increasing, $CO_2$ conversion and the selectivity of ethanol and $CH_4$ decrease while the selectivity of CO increases (Fig. S7†). Since $FeO_x$ could catalyze the reverse water-gas shift reaction (RWGS) to produce CO, the changes of $CO_2$ conversion and product distribution indicate that the excess Fe species has a passive effect on $CO_2$ conversion and ethanol synthesis by blocking the active Rh sites.[10] This blocking effect may be caused by the encapsulation of Rh sites by $FeO_x$ species, which have been proven by XPS measurements combined with CO chemisorption (Table S2†). On the other hand, the addition of Li can increase the $CO_2$ conversion of Rh/$TiO_2$ by 5%, while the selectivity of ethanol does not change (Fig. S6c†). Based on these results, we conclude the addition of Fe can promote the ethanol selectivity, while the addition of Li accelerates the $CO_2$ conversion as electronic promoter. As such, higher ethanol selectivity and $CO_2$ conversion are obtained by adding binary promoters *i.e.*, Fe and Li (Fig. S6d†).

More interestingly, we show the ethanol selectivity and $CO_2$ conversion over RhFeLi/$TiO_2$ NRs are much higher than that over RhFeLi/$TiO_2$ Com at 250°C (Fig. S7†). For example, 2.5 wt% RhFeLi/$TiO_2$ NRs (Rh:Fe:Li=1:1:1) catalyst presents more than 30% ethanol selectivity and 15% $CO_2$ conversion, which is about seven-fold higher for ethanol yield than 2.5 wt% RhFeLi/$TiO_2$ Com (Fig. 3). The catalytic performance of RhFeLi/$TiO_2$ NRs keeps stable in 20 h stability test (Fig. S7†). The superior reactivity and long-term stability of RhFeLi/$TiO_2$ NRs catalysts provide an inspiration for their potentially industrial application.

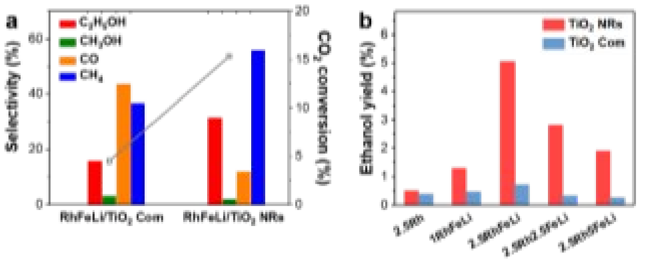

**Fig. 3.** (a) The $CO_2$ conversion (Grey) and the product selectivity of 2.5 wt% RhFeLi/$TiO_2$ NRs and 2.5 wt% RhFeLi/$TiO_2$ Com. (b) The ethanol yield of Rh-based catalyst supported on $TiO_2$ NRs and $TiO_2$ Com.

View Article Online
DOI: 10.1039/C8SC05608H

### Promotion effects of the hydroxyl

Firstly, the hydroxyl groups were introduced by pre-reduction of RhFeLi/$TiO_2$ NRs and RhFeLi/$TiO_2$ Com catalysts in $H_2$ atmosphere at 400°C. The fourier transform infrared (FTIR) experiments were carried out to characterize the surface hydroxyl groups on RhFeLi/$TiO_2$ catalysts. As shown in Fig. S8†, the broad band at 3450 $cm^{-1}$ and the sharp peak at 1640 $cm^{-1}$ are assigned to the stretching and bending vibrations of associative hydroxyls, respectively.[29] The density of hydroxyl groups on RhFeLi/$TiO_2$ NRs is much higher than that on RhFeLi/$TiO_2$ Com (Fig. 4a), suggesting that high-density hydroxyl groups could be introduced to catalytic system by using $TiO_2$ NRs. Subsequently, the catalytic properties of hydroxyls on $TiO_2$ NRs is characterized by CO temperature-programmed desorption (CO-TPD). A sharp signal peak of $CO_2$ (*m/z*=44) at ~ 0°C is observed in CO-TPD profiles for both RhFeLi/$TiO_2$ NRs and pure $TiO_2$ NRs (Fig. 4b, Fig. S8a†). As reported previously, the $CO_2$ may origin from water gas shift process, in which the CO adsorbed on Rh sites reacts with hydroxyl groups.[29-30] However, small $CO_2$ peak at ~ 0°C is observed over RhFeLi/$TiO_2$ Com and pure $TiO_2$ Com due to the lack of hydroxyls (Fig. 4c, Fig. S8a†).

The TOF of ethanol formed over RhFeLi/$TiO_2$ NRs is determined to be 0.12 $h^{-1}$, which is much higher than that over RhFeLi/$TiO_2$ Com or RhFeLi/$SiO_2$ (0.08 $h^{-1}$) (Table S2†). Therefore, we suggest that the surface hydroxyl may play an important role in ethanol formation via $CO_2$ hydrogenation. To verify the role of hydroxyls on ethanol formation, the RhFeLi/$TiO_2$ NRs catalyst was pre-treated in CO atmosphere (RhFeLi/$TiO_2$ NRs-CO). The removal process of hydroxyl groups

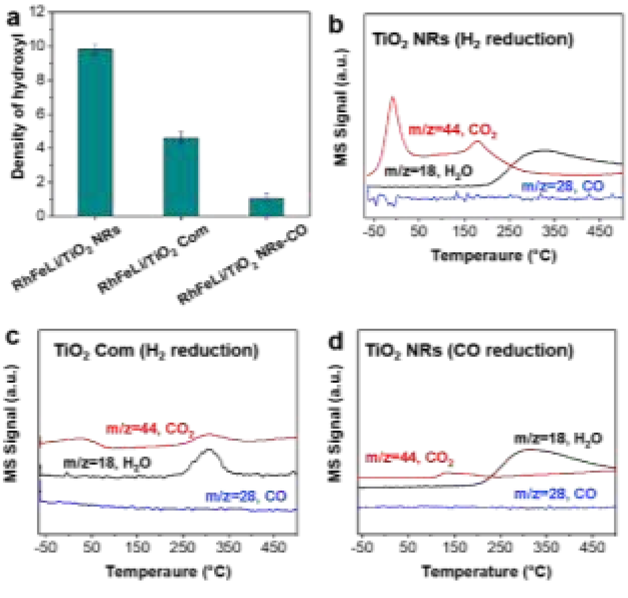

**Fig. 4.** (a) The peak area of hydroxyls in FTIR normalized by $S_{BET}$ (×$10^3$) over 2.5 wt% RhFeLi/$TiO_2$ NRs, 2.5 wt% RhFeLi/$TiO_2$ Com and 2.5 wt% RhFeLi/$TiO_2$ NRs-CO. (b) CO-TPD profiles of 2.5 wt% RhFeLi/$TiO_2$ NRs. Pretreatment: $H_2$ reduction at 400°C. (c) CO-TPD profiles of 2.5 wt% RhFeLi/$TiO_2$ Com. Pretreatment: $H_2$ reduction at 400°C. (d) CO-TPD profiles of 2.5 wt% RhFeLi/$TiO_2$ NRs. Pretreatment: CO reduction at 350°C.

View Article Online
DOI: 10.1039/C8SC05608K

in CO was monitored by *in situ* diffuse reflectance infrared fourier transform spectroscopy (DRIFTS, Fig. S9a†).[31] We find that the IR peak of hydroxyl stretching vibrations (3450 cm$^{-1}$) disappears gradually in CO at 350°C. The hydroxyls can be removed completely after ~ 12 minutes of CO-feeding (Fig. S9b †). After the pre-treatment in CO flow at 350°C, the $CO_2$ peak at ~ 0°C isn't observed in CO-TPD (Fig. 4d), and RhFeLi/$TiO_2$ NRs-CO catalysts with hydroxyl-deficient surface are prepared (Fig. 4a, Fig. S8b†). Compared with RhFeLi/$TiO_2$ NRs reduced with $H_2$, RhFeLi/$TiO_2$ NRs-CO catalyst performs much lower $CO_2$ conversion (4.7%) and produces almost no ethanol (Fig. 5a). The selectivity of CO reaches ~ 80% among the products and the selectivity of $CH_4$ decreases from 53.9% to 9.6%. In TEM images (Fig. S10†), RhFeLi/$TiO_2$ NRs and RhFeLi/$TiO_2$ NRs-CO catalysts show similar size distribution. Besides, there is no BE shift of XPS Rh 3d peak for RhFeLi/$TiO_2$ NRs-CO compared with RhFeLi/$TiO_2$ NRs (Fig. S11†, Table S4†). Therefore, the influences of size effect and chemical state of Rh can be excluded. Instead, the decrease of the selectivity of $CH_4$ and ethanol should be attributed to the lack of hydroxyls. When hydroxyl groups are re-introduced by $H_2$ exposure (Fig. 5b, Fig. S8b†), the promoted catalytic performance is achieved (35% ethanol selectivity and 18% $CO_2$ conversion), which is very similar with that over fresh RhFeLi/$TiO_2$ NRs reduced with $H_2$. These results further indicate hydroxyls play an important role in tuning product distribution and promoting ethanol synthesis through $CO_2$ hydrogenation.

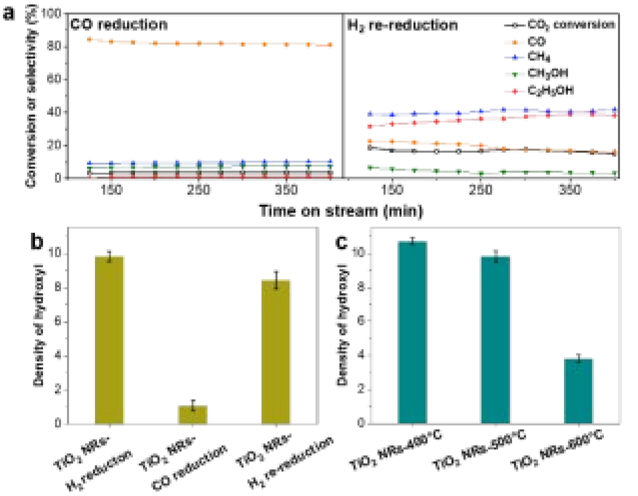

**Fig. 5.** (a) $CO_2$ conversion and product selectivity versus time obtained from 2.5 wt% RhFeLi/$TiO_2$ NRs. CO reduction was conducted at 350°C for 0.5 h. Re-reduction in $H_2$ was carried out at 400°C for 1 h. Reaction conditions: P = 30 atm, T = 250°C, GHSV= 6000 h$^{-1}$, $CO_2/H_2$ = 1/3. (b) The peak area of hydroxyls in FTIR normalized by $S_{BET}$ (×10$^3$) over 2.5 wt% RhFeLi/$TiO_2$ NRs pretreated under different reduction atmospheres. (c) The peak area of hydroxyls in FTIR normalized by $S_{BET}$ (×10$^3$) over 2.5 wt% RhFeLi/$TiO_2$ NRs calcined at different temperatures.

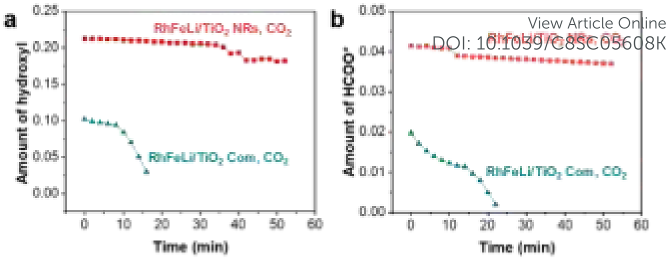

**Fig. 6.** (a) The absorbance intensity of hydroxls at 3600 cm$^{-1}$ in DRIFTS of 2.5 wt% RhFeLi/$TiO_2$ NRs and 2.5 wt% RhFeLi/$TiO_2$ Com versus time after switching the $CO_2$+$H_2$+Ar ($CO_2$:$H_2$=1:3) flow to pure $CO_2$ flow at 250°C. (b) The absorbance intensity of formate at 1595 cm$^{-1}$ in DRIFTS of 2.5 wt% RhFeLi/$TiO_2$ NRs and 2.5 wt% RhFeLi/$TiO_2$ Com versus time after switching the $CO_2$+$H_2$+Ar ($CO_2$:$H_2$=1:3) flow to pure $CO_2$ flow at 250°C.

In sequential experiments, the mixture of $CO_2$ and $H_2$ ($CO_2$:$H_2$=1:3) are firstly introduced to the *in situ* cell at 250°C, followed by a switch to pure $CO_2$ flow to investigate the stability of hydroxyls and formate species. In $CO_2$+$H_2$ atmosphere ($CO_2$:$H_2$=1:3) at 250°C, the bands at 3016, 2965 and 2880 cm$^{-1}$ in the $\nu_{C\text{-}H}$ region appear stemming from gaseous $CH_4$ (3016 cm$^{-1}$) and adsorbed formate species respectively. In the O-C-O stretching region between 1650 and 1200 cm$^{-1}$, the bands at 1520 and 1390 cm$^{-1}$ are assigned to carbonate, while the rest peaks may stem from adsorbed formate (1595, 1370 cm$^{-1}$, Table S5†).[32-34] The absorbance intensities of the dissociated hydroxyl stretching vibrations at 3600 cm$^{-1}$ and OCO asymmetric stretching vibration at 1595 cm$^{-1}$ in DRIFTS are used to represent the amount of hydroxyls and formate, respectively.[34] As shown in Fig. 6, the changes of the hydroxyl amount and the formate amount are plotted as a function of time when switching the $CO_2$+$H_2$ flow to pure $CO_2$ flow at 250°C. We find that the amounts of hydroxyls and formate species over RhFeLi/$TiO_2$ NRs keep almost unchanged under pure $CO_2$ flow within 40 mins (Fig. 6, Fig. S12a, c†). In contrast, the hydroxyls and formate adsorbed on RhFeLi/$TiO_2$ Com disappears rapidly within 20 min (Fig. 6, Fig. S12b, d†). We suggest that the abundant hydroxyl groups over RhFeLi/$TiO_2$ NRs can stabilize formate species, which has been proposed to be one of intermediates for methanation via formate hydrogenation and then scission of C-O in *$CH_x$-O.[18,35]

*In situ* DRIFTS was further carried out to investigate the catalytic role of hydroxyls in ethanol formation. In contrast to RhFeLi/$TiO_2$ Com, additional bands at 1470 cm$^{-1}$ and 1746 cm$^{-1}$ are observed on RhFeLi/$TiO_2$ NRs under $CO_2$+$H_2$ atmosphere ($CO_2$:$H_2$=1:3) at 250°C (Fig. 7a). The existence of the band at 1746 cm$^{-1}$ has been reported for Rh/$Al_2O_3$[35] and Ru/$Al_2O_3$[36] catalysts, which can be attributed to adsorbed formyl (CHO*) species. It is believed that the formation of CHO* is the rate-limiting step of ethanol synthesis (Scheme S1).[12] Also, CHO* is more favored to be dissociated into *$CH_x$ in thermodynamics than CO.[21-23,37] As expect, significant amounts of *$CH_3$ species (1470 cm$^{-1}$) are observed on the surface of RhFeLi/$TiO_2$ NRs (Fig. 7a).[17-18] Subsequently, these abundant adsorbed *$CH_3$ species on RhFeLi/$TiO_2$ NRs can be inserted by CO, which may be responsible for the high ethanol yield.[38] Based on the above analysis, a mechanism that hydroxyls stabilize the formate and accelerate the scission of $CH_x$-O to produce *$CH_3$ species is proposed (Scheme 1).

With increasing the calcination temperature from 400 to 600°C, the normalized peak area of associative hydroxyl vibration bands over RhFeLi/$TiO_2$ NRs decreases gradually, indicating the density of hydroxyls is decreased (Fig. 5c, Fig. S8c †). In addition, summed selectivity and TOF of $CH_4$ and ethanol show a downward trend with increasing the calcination

View Article Online
DOI: 10.1039/C8SC05608K

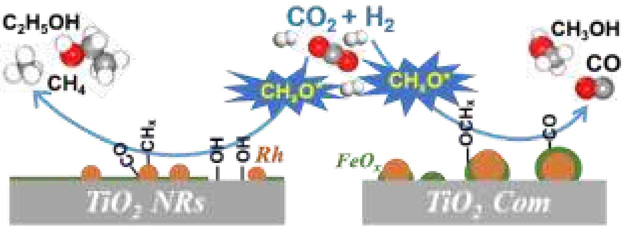

**Scheme 1.** Schematic of $CO_2$ hydrogenation over Rh-based catalyst with or without hydroxyl groups on $TiO_2$. The hydroxyls play an important role in accelerating the scission of $CH_x$-O* and promote the formation of ethanol.

temperature of $TiO_2$ NRs (Table S2 and S6†). Since the RhFeLi nanoparticles show similar size distribution (Fig. S10†) and same electronic state of Rh and Fe over $TiO_2$ NRs calcined at various temperatures (Fig. S11†, Table S4†), the differences in catalytic performance should be attributed to the changes of surface hydroxyls. It is noteworthy that the catalytic performance of RhFeLi/$TiO_2$ NRs-600°C is comparable to that of RhFeLi/$TiO_2$ NRs-CO catalyst, because there are few hydroxyls on their surfaces. Similarly, changing the support from $TiO_2$ NRs to $TiO_2$ Com can also generate hydroxyl-deficient surface, causing the selectivity of ethanol and $CH_4$ reduced largely (Table S6†). To display the relationship between hydroxyl groups and catalytic performance directly, we take the summed amount of $CH_4$ and ethanol as the total amount of $^*CH_3$, because these two products stem from $^*CH_3$ hydrogenation and CO insertion, respectively.[39] As shown in Fig. 7b, the amount of $^*CH_3$ exhibits linear correlation with the density of hydroxyls, illustrating hydroxyls may accelerate the scission of C-O bond to form $^*CH_3$ species.

The reactions of $CH_3OH$ and $H_2$ over RhFeLi/$TiO_2$ were conducted as well to elucidate the role of hydroxyls. The DRIFTS were obtained after pre-treatment with $CH_3OH$ and subsequent feeding with $H_2$ at 250°C (Fig. 7c). Upon the feeding of $CH_3OH$, all the samples show similar $CH_3O^*$ (2825, 2927 $cm^{-1}$) species.[40-42] After the feeding of $H_2$, the IR peak intensity of $CH_3O^*$ over RhFeLi/$TiO_2$ NRs decreases. Simultaneously, obvious IR peak of gaseous $CH_4$ (3016 $cm^{-1}$) can be observed over RhFeLi/$TiO_2$ NRs. The formation of $CH_4$ should be attributed to the C-O bond scission in $CH_3O^*$ followed by $^*CH_3$ hydrogenation. Hydroxyl groups over RhFeLi/$TiO_2$ NRs are suggested to promote the C-O bond scission in $CH_3O^*$ to produce $^*CH_3$ intermediate. On the contrary, the IR peak intensity of $CH_3O^*$ does not decrease, and $CH_4$ is hardly found over RhFeLi/$TiO_2$ Com and RhFeLi/$TiO_2$ NRs-CO after $H_2$ feeding. Therefore, it is reasonable to infer that hydroxyls on RhFeLi/$TiO_2$ NRs could protonate $CH_3O^*$, i.e., promoting C-O bond scission in $CH_3O^*$ to form $^*CH_3$. Similar phenomenon is observed under CO and $H_2$ at 250°C (Fig. 7d). The sharp $CH_4$ peak emerges on RhFeLi/$TiO_2$ NRs, which is accompanied by formate (2880, 2965 $cm^{-1}$) and $CH_3O^*$ (2825, 2927 $cm^{-1}$). In contrast, we find only $CH_3O^*$ species adsorbed over RhFeLi/$TiO_2$ NRs-CO. The IR peaks of gaseous $CH_4$ and formate are undetectable over RhFeLi/$TiO_2$ NRs-CO and RhFeLi/$TiO_2$ Com, which should be attributed to the removal of hydroxyls after CO treatment.

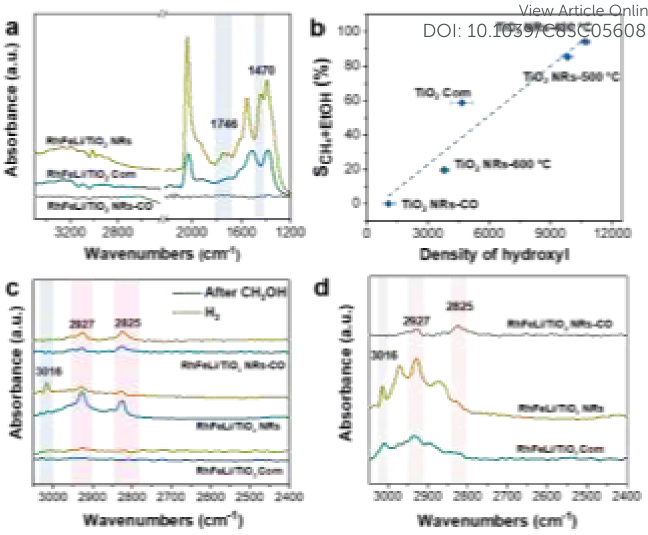

**Fig. 7.** (a) *In situ* DRIFTS over 2.5 wt% RhFeLi/$TiO_2$ NRs, 2.5 wt% RhFeLi/$TiO_2$ Com and 2.5 wt% RhFeLi/$TiO_2$ NRs-CO under $CO_2$+$H_2$+Ar ($CO_2$:$H_2$=1:3) atmosphere at 250°C. (b) The summed selectivity of $CH_4$ and ethanol as a function of the peak area of hydroxyls normalized by $S_{BET}$ of the samples obtained from 2.5 wt% RhFeLi supported on different $TiO_2$. (c) *In situ* DRIFTS over 2.5 wt% RhFeLi/$TiO_2$ NRs, 2.5 wt% RhFeLi/$TiO_2$ Com and 2.5 wt% RhFeLi/$TiO_2$ NRs-CO after $CH_3OH$+Ar adsorption followed by $H_2$ adsorption at 250°C. (d) *In situ* DRIFTS over 2.5 wt% RhFeLi/$TiO_2$ NRs, 2.5 wt% RhFeLi/$TiO_2$ Com and 2.5 wt% RhFeLi/$TiO_2$ NRs-CO under CO+$H_2$+Ar (CO:$H_2$ = 1:2) atmosphere at 250°C.

Previous works have proposed that ethanol can be synthesized by CO insertion into $^*CH_3$ species to form $CH_3CO^*$, followed by $CH_3CO^*$ hydrogenation.[37-38] To verify this route of ethanol formation, the DRIFTS of RhFeLi/$TiO_2$ NRs and RhFeLi/$TiO_2$ NRs-CO were obtained after pre-treatment with $CH_3OH$ and subsequent feeding with CO+$H_2$ (CO:$H_2$=1:1) at 250°C (Fig. S13a†). Both gaseous and liquid products were analyzed in the reaction of $CH_3OH$+CO+$H_2$ at 250°C (Fig. S13b†), and ethanol is the only $C_{2+}$ product. Hence, the appearance of methylene peak (2858 $cm^{-1}$) over RhFeLi/$TiO_2$ NRs indicates the C-C coupling and formation of ethanol.[43] However, the methylene, i.e., ethanol is not formed over RhFeLi/$TiO_2$ NRs-CO. According to these data, the high ethanol selectivity over RhFeLi/$TiO_2$ NRs might be attributed to the high-density hydroxyls, which enhances the C-O bond scission to produce $^*CH_x$ intermediates for the CO insertion.

Surface functionalization with hydroxyls is frequently applied to promote the catalytic performance of catalysts.[44-47] The role of surface hydroxyls has often been considered to modulate the local concentration of hydrophilic reactants, such as alcohols, around the active sites. For example, the hydrophobic treatment of Pd/MOF improves the catalytic activity of styrene hydrogenation by increasing the interaction between hydrophobic reactants and Pd sites.[48] In formaldehyde oxidation reaction, the abundant hydroxyl groups nearby the Pt active sites can also facilitate formate oxidation through the formation of Pt/Ni$(OH)_x$ interface.[49] In $CO_2$ hydrogenation reaction, hydroxyl groups on hydrophilic SiC quantum dots can promote the methanol formation via a H-transfer mechanism, in which the diffusion of H from hydroxyl groups to $CO_2$ assists the formation of intermediate $HCOO^*$.[50] Here, our work clearly demonstrates the catalytic role of hydroxyl groups in ethanol

View Article Online
DOI: 10.1039/C8SC05608K

synthesis via $CO_2$ hydrogenation. We show the surface hydroxyl species on RhFeLi/$TiO_2$ NRs can protonate methanol and reduce the energy barrier for C-O bond scission, facilitating the generation of *$CH_3$ species. Accordingly, abundant *$CH_3$ species can be inserted by CO obtained from RWGS to form $CH_3CO$*, followed by $CH_3CO$* hydrogenation to ethanol.

## Conclusions

In conclusion, we have demonstrated the crucial role of surface hydroxyls over the RhFeLi/$TiO_2$ NRs catalyst to synthesize ethanol from $CO_2$ hydrogenation. Based on in situ spectroscopic characterizations, we propose two advantages of $TiO_2$ NRs support for $CO_2$ hydrogenation to ethanol: (i) Rh-based nanoparticles are highly-dispersed on $TiO_2$ NRs due to the strong interaction between catalysts and $TiO_2$ NRs support, thus displaying high activity; (ii) abundant hydroxyls over $TiO_2$ NRs can protonate methanol, which is easily dissociated into *$CH_x$, thus favored the formation of ethanol upon CO insertion. This work not only provides the detailed understanding of the catalytic role of hydroxyls in heterogeneous catalysis but also opens an avenue for developing efficient catalysts for $CO_2$ conversion.

## Experimental section

### Chemicals

$TiO_2$ NRs were prepared by hydrothermal treatment of a mixture of titanium tetrachloride, nitric acid and water.[51-52] Briefly, titanium tetrachloride ($TiCl_4$, Shanghai Chemical Agent Co., 98%) was dissolved in ultrapure water within an ice-water bath to obtain the 3 M $TiCl_4$ solution. Subsequently, 35 mL aliquot of concentrated nitric acid ($HNO_3$, 15 M) was refluxed in a silicone oil bath and heated to 200°C gradually, and then 20 mL 3 M titanium tetrachloride solution was rapidly injected into nitric acid under vigorously stirring. After aging for 20 h, the autoclave was cooled to room temperature. The obtained precipitates were centrifuged and washed several times with deionized water and ethanol. The filtered solid was dried at 100°C in vacuum overnight and calcined at 300, 400, 500 and 600°C for 4 h, respectively (donated as $TiO_2$ NRs-x°C). Unless otherwise specified, $TiO_2$ NRs denoted $TiO_2$ NRs-500°C. The commercial $TiO_2$ ($TiO_2$ Com) was purchased from Alfa Aesar Chemical Co. ltd for comparison.

$RhCl_3$•n$H_2O$ (Huaweiruike Chemical Co., 99%), $LiNO_3$ (Alfa Aesar Chemical Co. ltd., 98%) and $Fe(NO_3)_3$•9$H_2O$ (Alfa Aesar Chemical Co. ltd., 98%) were used as precursors and a series of reducible metal oxides (MO) were used as the support. MO (1 g) were impregnated with distilled water (1 mL) containing the precursor by using ultrasonication for 1 h. Generally, the molar ratio of the Rh and promoters was 1:1 unless specified. Subsequently, the sample is dried at room temperature overnight and then at 80°C for 10 h. Finally, the sample is calcined in air at 300-500°C for 4 h and reduced in pure $H_2$ at 400°C for 2 h. The element loading was based on the weight ratio of Rh and Fe with respect to MO supports.

### Hydrogenation of $CO_2$

All the catalytic reactions were carried out in a fixed-bed micro-reactor. In a typical experiment, 300 mg of each catalyst with a 20-40 mesh size distribution was mixed with 2.0 g of quartz particles (SiC: granulation of 0.075-0.4 mm) to avoid hot spots and pressure drop across bed and packed in the stainless steel ($\phi$ 8 × 400 mm) tubular reactor. Prior to each experiment, the catalyst was activated by reducing in $H_2$ atmosphere (99.99%) with the flow rate of 30 mL/min and the temperature of 400°C for 1 h. The RhFeLi/$TiO_2$ NRs-CO sample was obtained from the RhFeLi/$TiO_2$ NRs-500°C reduced under CO flow at 350°C for 0.5 h. After the reduction of catalyst, the reactor was cooled down to reaction temperature. Then the reactant gases ($CO_2$ and $H_2$ with molar ratio of 1:3, 30 bar) were introduced into the reactor. The gas hourly space velocity (GHSV) was set at 6000 $h^{-1}$. The product gas was analyzed with an online gas chromatograph (GC, Agilent 7890B) equipped with two detectors. One is flame ionization detector (FID) with a HP-FFAP column using $H_2$ as a carrier gas to analyze the organic species such as alcohols, oxygenate and hydrocarbons. The other one is thermal conductivity detector (TCD) with columns of MS-5A column and Hayesep Q using He as a carrier gas to monitor the incondensable gas species including $H_2$, $CO_2$, $N_2$, CO and $CH_4$. All the flows between the reactor and the GC were heated and kept beyond 150°C, to avoid the liquefaction of the alcohols products.

## Conflicts of interest

There are no conflicts to declare.

## Acknowledgements

This work was financially supported by the National Key R&D Program of China (2016YFB0600901), the National Natural Science Foundation of China (21525626, 21603159, 21676181), the Program of Introducing Talents of Discipline to Universities (B06006) for financial support.

## References

1 M. Aresta, A. Dibenedetto and A. Angelini, *Chem. Rev.*, 2014, **114**, 1709-1742.
2 W. Wang, S. Wang, X. Ma and J. Gong, *Chem. Soc. Rev.*, 2011, **40**, 3703-3727.
3 H. Yang, C. Zhang and P. Gao, Wang, H.; Li, X.; Zhong, L.; Wei, W.; Sun, Y. *Catal. Sci. Technol.,* 2017, **7**, 4580-4598.
4 A. Swapnesh, V. C. Srivastava and I. D. Mall, *Chem. Eng. Tech.,* 2014, **37**, 1765-1777.
5 Z. He, Q. Qian, J. Ma, Q. Meng, H. J. Zhou, H. J. Song, Z. Liu and B. Han, *Angew. Chem. Int. Ed.,* 2016, **128**, 747-751.
6 D. L. S. Nieskens, D. Ferrari, Y. Liu and R, Kolonko, *Catal. Commun.,* 2011, **14**, 111-113.
7 T. Inui, T. Yamamoto, M. Inoue, H. Hara, T. Takeguchi and J. B. Kim, *Appl. Catal., a-Gen.,* 1999, **186**, 395-406.
8 M. Takagawa, A. Okamoto, H. Fujimura, Y. Izawa and H. Arakawa, *Stu. Sur. Sci. Catal.,* 1998, **114**, 525-528.

View Article Online
DOI: 10.1039/C8SC05608K

9 S. Li, H. Guo, C. Luo, H. Zhang, L. Xiong, X. Chen and L. Ma, *Catal. Lett*., 2013, **143**, 345-355.
10 H. Kusama, K. Okabe, K. Sayama and H. Arakawa, *Energy,* 1997, **22**, 343-348.
11 H. Kusama, K. Okabe, K. Sayama and H. Arakawa, *Catal. Today,* 1996, **28**, 261-266.
12 Y. Choi and P. Liu, *J. Am. Chem. Soc.,* 2009, **131**, 13054-13061.
13 N. Yang, A. J. Medford, X. Liu, F. Studt, T. Bligaard, S. F. Bent and J. K. Norskov, *J. Am. Chem. Soc.,* 2016, **138**, 3705-3714.
14 Y. Wang, H. Luo, D. Liang and X. Bao, *J. Catal.,* 2000, **196**, 46-55.
15 R. G. Zhang, M. Peng and B. J. Wang, *Catal. Sci. Tech.,* 2017, **7**, 1073-1085.
16 J. C. Matsubu, V. N. Yang and P. Christopher, *J. Am. Chem. Soc.,* 2015, **137**, 3076-3084.
17 S. Kattel, W. Yu, X. Yang, B. Yan, Y. Huang, W. Wan, P. Liu and J. G. Chen, *Angew. Chem. Int. Ed.,* 2016, **55**, 7968-7973.
18 S. Kattel, P. Liu and J. G. Chen, *J. Am. Chem. Soc.,* 2017, **139**, 9739-9754.
19 D. Wang, Q. Bi, G. Yin, W. Zhao, F. Huang, X. Xie and M. Jiang, *Chem. Commun.,* 2016, **52**, 14226-14229.
20 S. Bai, Q. Shao, P. Wang, Q. Dai, X. Wang and X. Huang, *J. Am. Chem. Soc.,* 2017, **139**, 6827-6830.
21 R. Burch and M. J. Hayes, *J. Catal.,* 1997, **165**, 249-261.
22 J. Xu, X. Su, H. Duan, B. Hou, Q. Lin, X. Liu, X. Pan, G. Pei, H. Geng, Y. Huang and T. Zhang, *J. Catal.,* 2016, **333**, 227-237.
23 R. Zhang, B. Wang, H. Liu and L. Ling, *J. Phy. Chem. C,* 2011, **115**, 19811-19818.
24 J. Lee, D. C. Sorescu and X. Y. Deng, *J. Am. Chem. Soc.,* 2011, **133**, 10066−10069.
25 L. Liu, C. Zhao and Y. *J.* Li, *Phy. Chem. C,* 2012, **116**, 7904-7912.
26 J. Z. Y. Tan, Y. Fernández, D. Liu, M. Maroto-Valer, J. Bian and X. Zhang, *Chem. Phys. Lett.,* 2012, **531**, 149-154.
27 J. C. Matsubu, S. Zhang, L. DeRita, N. S. Marinkovic, J. G. Chen, G. W. Graham, X. Pan and P. Christopher, *Nat. Chem.,* 2017, **9**, 120-127.
28 T. Huizinga, H. F. J. van 'T Blik, J. C. Vis and R. Prins, *Surf. Sci.,* 1983, **135**, 580-596.
29 Z. Xu, J. Yu, and M. Jaroniec, *Appl. Catal., B,* 2015, **163**, 306-312.
30 T. Yang, Y. Huo, Y. Liu, Z. Rui and H. Ji, *Appl. Catal.,* B, 2017, **200**, 543-551.
31 X. Zou, Z. Rui, S. Song and H. Ji, *J. Catal*., 2016, **338**, 192-201.
32 J. Graciani, K. Mudiyanselage, F. Xu, A. E. Baber, J. Evans, S. D. Senanayake, D. J. Stacchiola, P. Liu, J. Hrbek, J. Fernandez Sanz and J. A. Rodriguez, *Science*, 2014, **345**, 546-550.
33 X. Wang, Y. Hong, H. Shi and J. Szanyi, *J. Catal*., 2016, **343**, 185-195.
34 X. Wang, H. Shi and J. Szanyi, *Nat. Commun.,* 2017, **8**, 513.
35 D. Heyl, U. Rodemerck and U. Bentrup, *ACS Catal*., 2016, **6**, 6275-6284.
36 P S. Eckle, H.-G. Anfang and R. J. r. Behm, *J. Phy. Chem. C,* 2011, **115**, 1361-1367.
37 R. Zhang, G. Wang, B. Wang and L. Ling, *J. Phy. Chem. C,* 2014, **118**, 5243-5254.
38 Y. H. Zhao, K. Sun, X. Ma, J. Liu, D. Sun, H. Y. Su and W. X. Li, *Angew. Chem. Int. Ed. Engl.,* 2011, **50**, 5335-5338.
39 G. Prieto, P. Concepción, A. Martínez and E. Mendoza, *J. Catal.,* 2011, **280**, 274-488.
40 J. Wang, G. Li, Z. Li, C. Tang, Z. Feng, H. An, H. Liu, T. Liu and C. Li, *Sci. Adv.,* 2017, **3**, e1701290.
41 I. A. Fisher and A. T. Bell, *J. Catal*., 1997, **172**, 222-237.
42 A. Goguet, F. C. Meunier, D. Tibiletti, J. P. Breen and R. Burch, *J. Phy. Chem. B,* 2004, **108**, 20240-20246.
43 M. A. Natal-Santiago and J. A. Dumesic, *J. Catal*., 1998, **175**, 252-268.
44 Y. Dai, S. Liu and N. Zheng, *J. Am. Chem. Soc.,* 2014, **136**, 5583-5586.
45 Q. Sun, B. Aguila, G. Verma, X. Liu, Z. Dai, F. Deng, X. Meng, F.-S. Xiao and S. Ma, *Chem,* 2016, **1**, 628-639.
46 F. Liu, W. Kong, C. Qi, L. Zhu and F.-S. Xiao, *ACS Catal.,* 2012, **2**, 565-572.
47 J.-D. Lin, Q.-Y. Bi, L. Tao, T. Jiang, Y.-M. Liu, H.-Y. He, Y. Cao, and Y.-D. Wang, *ACS Catal*., 2017, **7**, 1720-1727.
48 G. Huang, Q. Yang, Q. Xu, S. Yu and H. Jiang, *Angew. Chem. Int. Ed.,* 2016, **55**, 7379-7383.
49 T. Yang, Y. Huo, Y. Liu, Z. Rui and H. Ji, *Appl. Catal., B,* 2017, **200**, 543-551.
50 Y. H. Peng, L. B. Wang, Q. Q. Luo, Y. Cao, Y. Z. Dai, Z. L. Li, H. L. Li, X. S. Zheng, W. S. Yan, J. L. Yang and J. Zeng, *Chem,* 2018, **4**, 613-625.
51 Q. Huang and L. Gao, *Chem. Lett.,* 2003, **32**, 638-639.
52 Q. Zhang and L. Gao, *Langmuir,* 2003, **19**, 967-971.